Int. J. Heat Mass Transfer. Vol. 32, No. 8, pp. 1575–1580, 1989
Printed in Great Britain

0017–9310/89 $3.00 + 0.00

Spectral emissivity measurement

K. S. DOMINGUEZ and J. R. WYNNYCKYJ
Department of Chemical Engineering, University of Waterloo, Waterloo, Ontario, Canada N2L 3G1

(*Received* 9 *September* 1988 *and in final form* 17 *January* 1989)

Abstract—New methods to measure high-temperature thermophysical properties of porous spheres have been reported recently. A refinement in the emissivity measurement is described here. A pellet is equilibrated in a black body enclosure and then rapidly isolated by momentarily moving a non-reflective shield over it. Systems-dynamics theory is applied to separate the instrument response from the true radiant flux. Advantages over the previous approach are shown. Spectral emissivities of partly-oxidized magnetite pellets in the spectral range $1.48 < \lambda < 1.80$ μm are reported.

INTRODUCTION

A NEW METHOD to measure the band or spectral emissivity of porous spheres has been described recently [1]. It is part of an integrated approach to measure the total emissivity and the effective thermal conductivity of pellets in their 'as is' state [2]. Accurate data of this type are required in modelling high-temperature chemical and metallurgical processes. The methods are rapid and involve very simple apparatus. The processing of the experimental outputs into the actual thermophysical-property values, however, is rather involved. This paper reports on an improvement recently developed to evaluate the spectral emissivity from the experiment. Also, complete software packages have been developed to evaluate all three properties, and these are given elsewhere [3].

The principle of the new emissivity method is as follows: a pellet, in thermal equilibrium with its surroundings and radiating as a black body, is suddenly isolated by a cold, non-reflecting shield. It now radiates as if into free space. Were the radiant flux of the pellet to be monitored by a spectral pyrometer, both before and during isolation, the ideal response should be as shown in Fig. 1(a). Section A represents the black body emission and section B the isolated, free-space emission. The emissivity is the ratio of the two fluxes. In practice, however, the pellet begins to cool rapidly, immediately upon isolation from the furnace wall. As well, the measurement 'system' does not have an instantaneous response. The system comprises the pyrometer, with a millivolt output, and a differential voltage chart recorder to read the output. In addition, there is the physical process of sliding the shield over the pellet.

Figure 1(b) is an example of a typical experimental output. Portion A still represents the black body emission, while portion B clearly shows the effects of cooling and of instrument response lags. In order to determine the spectral emissivity an accurate flux measurement at the instant that the pellet is isolated is required. This is point C of Fig. 1(b).

In the original study [1], the approach taken to obtain this zero-time value was to model section B of the curve in Fig. 1(b), after sufficient time had elapsed to assume that the system was free of instrument time lags, and to extrapolate the curve to zero time.

The equations describing the cooling curve, section B, are given as equations (1)–(5) in Table 1. Equation (1) is the solution to Fourier's second law for the surface temperature, assuming a constant heat transfer coefficient. Even with the latter simplification, this equation involves a very complex series solution. A simpler formalism to describe this curve was, therefore, used in the original study [1] and is given as equation (6) in Table 1. The exponential form was chosen arbitrarily, the choice resulted in the least error in the spectral emissivity, as described in the aforementioned study [1]. This curve was extrapolated back to zero time to obtain the flux at the instant the pellet was isolated. Equation (7) was used to obtain the spectral emissivity.

This procedure may be subject to the intrinsic errors arising from extrapolating into a region of steep gradients an arbitrarily chosen formalism fitted to data in a less steep region. A second approach, therefore, has been developed and is the subject of this paper.

BASIS OF THE METHOD

In the new approach, the response dynamics of the system are determined in a separate experiment. The data from this experiment are fitted to a second-order overdamped transfer function [4]. The overall output curve from an emissivity experiment, such as Fig. 1(b), is then corrected for the system response. The details of the method are described next and the equations pertaining to the method are listed in Table 2.

The combined function, equivalent to equation (6) of the old method, is equation (13) in Table 2. This is

NOMENCLATURE

A	area under curve, Fig. 3 [s]
a	constant in equations (10) and (11) [mV]
B	slope of tangent to point of inflection, Fig. 3 [s^{-1}]
b	constant in equations (10) and (11) [$mV\,s^{-1}$]
c	constant in equations (10) and (11), $m(t)$ [$mV\,s^{-2}$]
C_p	heat capacity of pellet [$J\,kg^{-1}\,K^{-1}$]
C_i	fractional output at point of inflection, Fig. 3 [—]
$C(t)$	output curve, equation (13) [mV]
d, f	constants determined from a fit to experimental data; used in equation (6) [$mV\,s^{-1}$]
E	correction factor for reflected radiation from shield, equation (8) [—]
F_2-F_1	fraction of the total radiant energy of a black body in the wavelength interval of a pyrometer
g	constant determined from a fit to experimental data; used in equation (6) [s^{-1}]
I_{pyro}	flux recorded by pyrometer [$W\,m^{-2}$]
I_{black}	black body flux [$W\,m^{-2}$]
k_e	effective thermal conductivity of the pellet [$W\,m^{-1}\,K^{-1}$]
L	system dead time [s]
L_T	length of hot zone in furnace tube [m]
$m(t)$	input curve, equation (10) [mV]
m	inverse Biot number [—]
M, Q, R	constants determined from a fit to experimental data; used in equation (13) [mV]
N	constant determined from a fit to experimental data; used in equation (13) [$mV\,s^{-1}$]
P	constant determined from a fit to experimental data; used in equation (13) [$mV\,s^{-2}$]
R_p	radius of pellet [m]
R_T	radius of tube [m]
T_1, T_2	process constants [s]
$T_R(t)$	time-dependent surface temperature of pellet [K]
T_S	shield temperature [K]
T_I	initial pellet temperature [K]
U	overall heat transfer coefficient [$W\,m^{-2}\,K^{-1}$].

Greek symbols

$\varepsilon_{\Delta\lambda}$	spectral emissivity ofpellet [—]
$\varepsilon^s_{\Delta\lambda}$	spectral emissivity of shield [—]
$\theta(t)$	dimensionless temperature [—]
τ	dimensionless time, Fourier number [—]
ψ_n	parameter in infinite series solution, equation (1).

a product of two functions. The first, equation (10), is assumed to give the true flux reaching the pyrometer, i.e. free from any influence of slow instrument response. This is henceforth called the input function, $m(t)$. The second function is the system-response function $G(s)$ [4], given by equation (9). To obtain equation (13), the input function is first transformed from the real-time domain into the Laplace domain, resulting in equation (11), where s is the Laplace parameter [4]. Equation (12) is the product of $G(s)$ and $m(s)$, equations (9) and (11), both in the Laplace domain. Following the use of the auxiliary parameters, defined in Table 3, equation (12) is then converted back into the real-time domain, to give equation (13).

The theoretical equation for the cooling curve, equation (1), is much too cumbersome for the Laplace transformation required in this analysis. A simpler formalism was again required. The second-order poly-

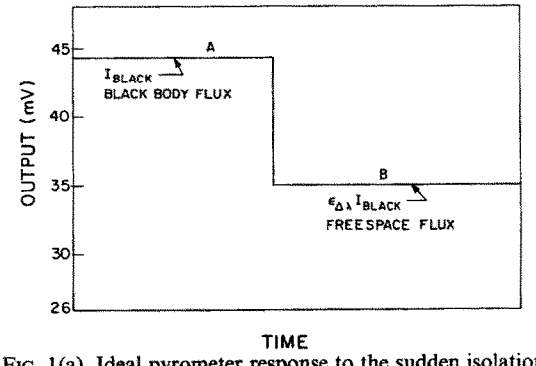

FIG. 1(a). Ideal pyrometer response to the sudden isolation of a sphere, initially in thermal equilibrium with a black body enclosure.

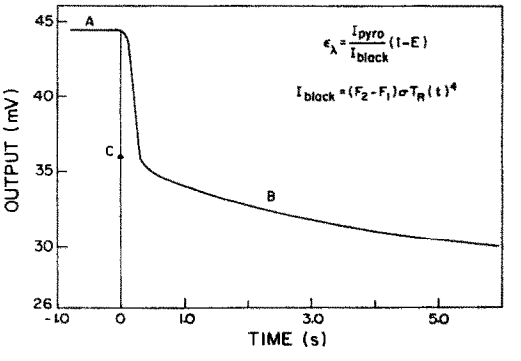

FIG. 1(b). Typical pyrometer response in the emissivity experiment.

Table 1. Equations pertaining to the description of the emissivity experiment

$$\theta(t) = 2\sum_{n=1}^{\infty} \frac{\sin\psi_n - \psi_n\cos\psi_n}{\psi_n - \sin\psi_n\cos\psi_n}\frac{\sin\psi_n}{\psi_n}\exp(-\psi_n^2\tau) \quad (1)$$

$$\psi_n\cot\psi_n = 1 - 1/m \quad (2)$$

$$m = \frac{k_c}{UR_p} \quad (3)$$

$$\theta(t) = \frac{T_R(t) - T_S}{T_I - T_S} \quad (4)$$

$$\tau = \frac{k_c}{\rho C_p R_p^2}t \quad (5)$$

$$C(t) = d + f\exp(-gt) \quad (6)$$

$$\varepsilon_{\Delta\lambda} = \frac{I_{pyro}}{I_{black}}(1-E) \quad (7)$$

$$E = (1-\varepsilon_{\Delta\lambda})(1-\varepsilon^s_{\Delta\lambda})\left\{\frac{4R_p^2L_T}{R_T(L_T^2+4R_T^2)}\right\} \quad (8)$$

Table 2. Equations relating to transfer function analysis

$$G(s) = \frac{e^{-Ls}}{(T_1s+1)(T_2s+1)} \quad (9)$$

$$m(t) = a + bt + ct^2 \quad (10)$$

$$m(s) = a/s + b/s^2 + 2c/s^3 \quad (11)$$

$$C(s) = \frac{1}{T_1T_2}[a/s + b/s^2 + 2c/s^3]\frac{e^{-Ls}}{(s+1/T_1)(s+1/T_2)} \quad (12)$$

$$C(t) = M + N(t-L) + P(t-L)^2 + Q\,e^{-(t-L)/T_1} + R\,e^{-(t-L)/T_2} \quad (13)$$

nomial, as given in equation (10), was chosen based on the fact that it fits equation (1) very well in the range of interest, as shown in Fig. 2. Equation (1), evaluated for three values of the inverse Biot number m, is plotted in Fig. 2 as a series of point symbols. Instead of dimensionless temperature, the result is given directly in millivolts of pyrometer output against real time. These results were obtained by substituting $\theta(t)$ from equation (1) into the Stefan–Boltzmann law for the spectral interval $F_2 - F_1$ of the pyrometer

$$I_{pyro} = \sigma(F_2 - F_1)[\theta(T_I - T_S) + T_S]^4. \quad (19)$$

The standard calibration curve supplied by the manufacturer for the G-series pyrometer was used to convert the calculated I_{pyro} values into pyrometer millivolts.

The negative values for the $m = 0.02$ curve in Fig. 2 arise from the fact that the pyrometer millivolt output goes to zero when the source temperature is 350°C. The inverse Biot number appropriate for the present experimental conditions is in the vicinity of 0.18. The values of T_I, T_S, and of the parameters used in this calculation are listed in Table 4.

Next the polynomial $m(t)$ was fitted to the symbol curves using a Lotus 123 software package [5] and the

Table 3. Relationships between constants in Table 2

$$a = M + N(T_2 + T_1) + 2P(T_1T_2) \quad (14)$$
$$b = N + 2P(T_2 + T_1) \quad (15)$$
$$c = P \quad (16)$$
$$Q = [M + NT_2]T_1/(T_2 - T_1) \quad (17)$$
$$R = [M + NT_1]T_2/(T_1 - T_2) \quad (18)$$

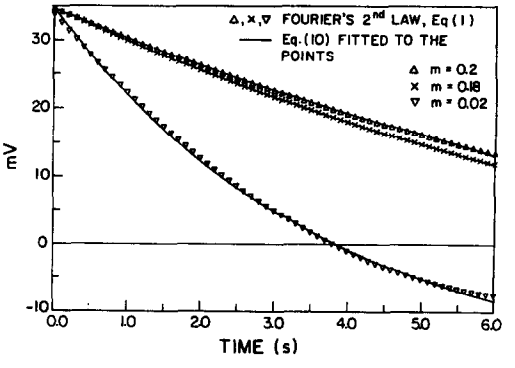

FIG. 2. Comparison of the form of the functions: Fourier's second law for the surface temperature with equation (10).

Table 4. Parameters for the calculation of Fig. 2

(a) Values for equation (1)

$C = 976.5\ \text{J kg}^{-1}\ \text{K}^{-1}$	$T_I = 773\ \text{K}$
$\rho = 5310\ \text{kg m}^{-3}$	$T_S = 333\ \text{K}$
$R_p = 6\ \text{mm}$	$k_c = 0.3\ \text{W m}^{-1}\ \text{K}^{-1}$

(b) Best fit values of constants in equation (10)

m	a	b	c
0.02	33.73	−12.32	0.906
0.18	34.59	−4.82	0.173
0.2	34.64	−4.45	0.155

constants a, b and c were evaluated. The values of these constants are listed in Table 4 and the corresponding curves are plotted as solid curves in Fig. 2. The excellent agreement suggests that the second-order polynomial, equation (10), is a valid model of the cooling curve.

EVALUATION OF THE SYSTEM RESPONSE FUNCTION, $G(s)$

The systems response function, equation (9), contains constants T_1, T_2 and L. These are evaluated in a separate experiment, as follows. The pyrometer is sighted on a pellet under black body conditions, e.g. section A in Fig. 1. Next, the pyrometer view is blocked by rapidly placing a piece of cold, white paper in front of the pyrometer lens. The output before and during the blockage is recorded by the same instrumentation as in the spectral emissivity experiment. This blockage of the pyrometer sight effectively results in the application of a step input to the process equipment. Figure 3 is a typical output obtained from this experiment.

To evaluate the constants T_1, T_2 and L, the output was analyzed using a method developed by Sundaresan *et al.* [6]. In this approach, the slope B at the point of inflection, the point of intersection of the tangent at the point of inflection with the abscissa, t_m, and the area A (all in Fig. 3), are required. The traditional Oldenburger method [7] requires a value of the fractional output at the point of inflection. Due to the difficulty in accurately determining the point of inflection in a rapid transient response, the former approach was preferred over the latter.

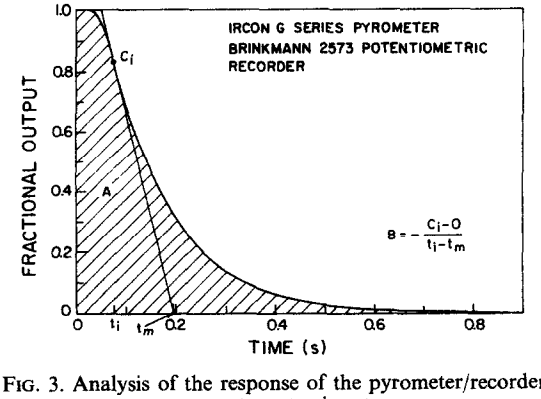

FIG. 3. Analysis of the response of the pyrometer/recorder system to a step input.

An Ircon Series G pyrometer and a Brinkmann 2573 potentiometric recorder were used in this work. The pyrometer is sensitive in the spectral range 1.48–1.80 μm. The values of the parameters in Fig. 3 for this instrument system have been determined and are listed in Table 5, column (i). Using these values, the parameters T_1, T_2, and L were estimated by following in detail the procedure described by Sundaresan *et al.* They are listed in Table 5, column (ii).

RESULTS

An experimental result from an emissivity measurement is given in Fig. 4 as a series of diamond points. This is a computer rendition of the digitized values of a recorder trace. The result is for a pellet made by balling a finely powdered magnetite concentrate [8] and then partially oxidizing the pellet. The constants M, N and P were evaluated by fitting equation (13) to the experimental trace using the same Lotus 123 package described earlier [5]. Their values are given in Table 5, column (iii). A curve calculated using these values is plotted in Fig. 4 as a solid line. The fit is seen to be very good. The values of the constants a, b and c were then calculated using equations (14)–(16), respectively, and are listed in Table 5, column (iv). Figure 5 is a plot of the input function $m(t)$, equation (10), with the values of a, b and c as listed in Table 5. Note that the required intersection point $\varepsilon_{\Delta\lambda} I_{\text{black}}$ is given directly as the value of a in Table 5, and is 35 mV.

Currently, the spectral emissivity of magnetite-concentrate pellets from the Griffith Mine is being studied [9]. Some results for a range of degrees of oxidation of magnetite to haematite are shown in Table 6. The effect of added bentonite, a binder, is also shown. All experiments have been performed at 500°C. The emissivities have been evaluated using equation (7), whereby the factor E was neglected. This factor corrects for the reflected radiation from the shield walls, equation (8). For the experimental apparatus used the value of E is less than 0.007 [1]. For a magnetite pellet oxidized to 83.5% and containing no bentonite the spectral emissivity, measured at 500°C, is 0.613. The only data for the spectral emissivity of pure haematite in the wavelength band of this experiment seems to be at 1000°C, as given by Touloukian [10]. It is 0.63, in very good agreement with our result.

CONCLUDING REMARKS

An important issue in the emissivity method is to obtain an unambiguous value of the radiant flux at the instant when the pellet is isolated from the black body enclosure. The new method discussed in this paper

Table 5. Values of constants in equations (9), (10) and (13)

(i) $G(s)$	(ii)	(iii) $C(t)$	(iv) $m(t)$
$A = 0.175$	$T_1 = 0.11706$	$M = 35.159$	$a = 34.989$
$t_m = 0.199$	$T_2 = 0.02844$	$N = -1.326$	$b = -1.303$
$B = 5.425$	$L = 0.02997$	$P = 0.079$	$c = 0.079$

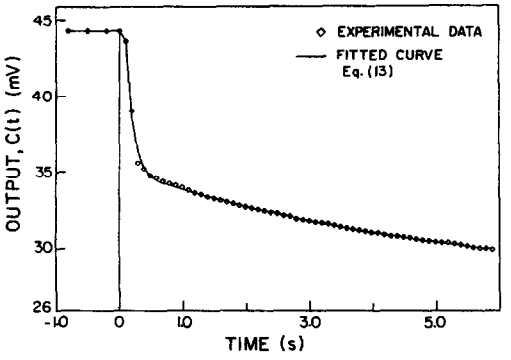

FIG. 4. Fit of input curve and transfer function to experiment.

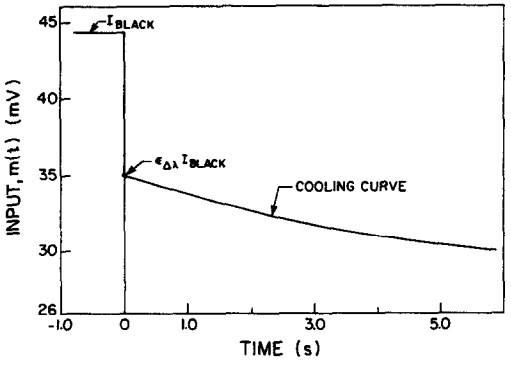

FIG. 5. Input curve, $m(t)$, evaluated from experimental data; 83.5% oxidized magnetite pellet.

Table 6. Measured spectral emissivity of oxidized pellets made from magnetite powder

Percentage oxidation	Bentonite addition	Spectral emissivity, $\epsilon_{\Delta\lambda}$ $(1.48 < \lambda < 1.8)$
46.9†	no	0.830
52.2†	no	0.769
69.8†	no	0.722
83.5†	no	0.613
85.8‡	2%	0.536
85.1‡	2%	0.520
86.3‡	2%	0.534
86.7‡	2%	0.518

† Oxidized at 500°C to 52% completion, 700°C to 70% completion and 850°C to 83.5% completion.
‡ Oxidized at 850°C.

provides a significant improvement over what has been previously published. The very-fast-response instrumentation is, moreover, no longer required. Instrument time lags are now incorporated into the analysis and are quantitatively accounted for. This is an important additional benefit.

The effect of the time lag of the shield movement is dealt with as follows. By varying the speed of shield movement, the point at which this speed becomes a factor can be detected as a change in the slope of the early portion of the output curve in Fig. 4. With practice, the experimenter can thrust the shield into the furnace at a high enough speed such that the resultant slope is equal to that obtained in the step function experiment (Fig. 3).

A second-order, overdamped transfer function was found to best model the process dynamics of the pyrometer/recorder system. The second-order polynomial is an adequate representation of the theoretical cooling curve, as predicted by Fourier's second law, and results in a good fit betwen the experimental data and the output curve, $C(t)$. Finally, the experimental values of the emissivity of iron ore pellets compare favourably with those listed in the literature.

Acknowledgements—Financial support for this work was from the Natural Sciences and Engineering Research Council of Canada from Operating and Strategic grants to J. R. Wynnyckyj. The authors thank E. P. Wonchala for several suggestions in connection with the modelling of the systems dynamics and J. Slusarczyk for help with the apparatus.

REFERENCES

1. S. K. Barua, J. R. Wynnyckyj and W. J. Rankin, Measurement of band emissivity of porous spheres at high temperatures, *Can J. Chem. Engng* **65**, 329–334 (1987).
2. S. K. Barua and J. R. Wynnyckyj, Measurement of high-temperature effective thermal conductivity of porous spheres, *Can. J. Chem. Engng* **64**, 695–701 (1986).
3. K. Dominguez and J. R. Wynnyckyj, Measurement of thermophysical properties of porous spheres at high temperatures, computer software applications, *Proc. Int. Symp. on Computer Software in Chemical and Extractive Metallurgy* (Edited by W. T. Thompson, F. Ajersch and G. Eriksson), pp. 269–284. Pergamon Press, Oxford (1988).
4. G. Stephanopoulos, *Chemical Process Control*, p. 215. Prentice-Hall, Englewood Cliffs, New Jersey (1984).
5. Lotus 123, Lotus Development Corporation (1982).
6. K. R. Sundaresan, C. Chandra Prasad and P. R. Krishnaswamy, Evaluating parameters from process

transients, *Ind. Engng Chem. Process Des. Dev.* **17**(3), 237–241 (1978).
7. R. C. Oldenburger, *The Dynamics of Automatic Controls*, p. 276. ASME, New York (1948).
8. D. Zaharchuk, An investigation of the strength of agglomerates using mercury porosimetry. MASc thesis, University of Waterloo (1985).
9. J. R. Wynnyckyj, The correlation between the strength factor and the true tensile strength of agglomerate spheres, *Can. J. Chem. Engng* **63**, 591–597 (1982).
10. Y. S. Touloukian (Editor), Thermal radiative properties. In *Thermophysical Properties of Matter*, Vol. 8, pp. 281–282. Plenum, New York (1970).

MESURE DE L'EMISSIVITE SPECTRALE

Résumé—De nouvelles méthodes de mesure des propriétés thermophysiques à haute température de sphères poreuses ont été présentées récemment. Un perfectionnement de la mesure de l'émissivité est décrit ici. Un boulet est en équilibre dans une cavité de corps noir et il est isolé rapidement par un écran non réflecteur. La théorie dynamique des systèmes est appliquée pour séparer la réponse de l'instrument du flux radiatif réel. On montre les avantages sur les approches antérieures. On présente les émissivités spectrales des boules de magnétite partiellement oxydées, pour le domaine $1{,}48 < \lambda < 1{,}80$ μm.

MESSUNG VON SPEKTRALEN EMISSIONSKOEFFIZIENTEN

Zusammenfassung—Vor kurzem wurden neue Methoden zur Bestimmung thermophysikalischer Eigenschaften poröser Kugeln bei hohen Temperaturen veröffentlicht. Hier wird eine Verfeinerung der Methode zur Messung des Emissionskoeffizienten beschrieben. Ein Pellet, das im Strahlungsgleichgewicht mit einer schwarz strahlenden Umgebung ist, wird durch das plötzliche Einbringen eines nicht-reflektierenden Strahlungsschildes aus dem Gleichgewicht gebracht. Die Theorie der System-Dynamik wird angewandt, um das Antwortverhalten des Meßgeräts vom tatsächlichen Strahlungsfluß zu separieren. Die Vorteile gegenüber der früheren Methode werden aufgezeigt. Die spektralen Emissionskoeffizienten teilweise oxidierter Magnetit-Pellets im Wellenlängenbereich $1{,}48 < \lambda < 1{,}8$ μm werden vorgestellt.

ИЗМЕРЕНИЕ СПЕКТРАЛЬНОЙ ИЗЛУЧАТЕЛЬНОЙ СПОСОБНОСТИ

Аннотация—В последнее время предложены новые методы измерения высокотемпературных теплофизических свойств пористых сфер. В данной работе уточнена методика таких измерений. Внутри абсолютно черной полости в равновесии с ней находится шарик, который мгновенно изолируется неотражающим экраном. Разделение отклика прибора и истинного значения лучистого потока рассчитывается по теории динамики систем. Показаны преимущества перед методом, применявшемся ранее. Даны значения спектральных излучательных способностей частично окисленных шариков магнетита в диапазоне $1.48 < \lambda < 1.80$ мкм.